Seismic Potential Forecasting in a Deep Longwall Mine

Z. Khademian
CDC NIOSH, Pittsburgh Mining Research Division

J. Beale
Pilot Geophysical LLC

S. Hicks, J. Fuller, Q. Justice
Coronado Global Resources, Inc.

Z. Agioutantis
University of Kentucky

ABSTRACT

Seismic events can be induced by mining due to unstable rock failures or slips along geologic structures leading to the sudden release of strain energy stored within the rock near underground openings. Depending on their intensity and proximity to the working area, seismic events may raise safety concerns, and thus the forecasting of the seismic potential in advance of mining can mitigate safety hazards. The integration of seismic data into geomechanical modeling can provide a tool for identifying areas with elevated potential for seismic activity. In previous works, a methodology was developed to forecast seismic potentials in a pseudo-2D geomechanical model. In this paper, seismic events, ranging in magnitude from about -1.0 M_L to 3.7 M_L, recorded in a deep longwall mine (> 450 m) in Virginia during mining of six adjacent panels, were evaluated to identify areas where larger magnitude events (> 1 ML) had occurred. A three-dimensional geomechanical model of the same area was constructed in the 3DEC software to calculate the state of energy in the system with the progress of mining along the entire length of each panel. The variation in the energy content of the model was monitored, and zones with potentially damaging events with compression-type and slip-type signatures were identified by defining a Seismic Potential Index (SPI). The results show that slip-type events along bedding planes followed by compressive-type events in the sandstone roof are the mechanism for large seismic events in the studied mine. The locations of anomalous events corresponded to the regions where both compression-type SPI (C-SPI) and slip-type SPI (S-SPI) were elevated. The modeling results were compared with the recorded seismic events to evaluate the model performance in forecasting the seismic potentials. The model was able to forecast 100% of regions with elevated and moderate seismic potential and 89% of regions with low seismic potential. This shows the applicability of energy balance calculations for forecasting the approximate location and timing of destructive seismic events in advance of mining.

INTRODUCTION

Mining-induced seismicity has long been a subject of research in underground mining because the unpredictable nature of these events and their proximity to the working area raise concerns for the health and safety of the mining workforce. To this end, seismic monitoring has become a part of mining safety practices, but the correlation between mining parameters, geology, and destructive events is poorly understood. The repeating experience from injuries, fatalities, and loss of capital caused by destructive seismic events show the gap in knowledge and relevant technologies for analyzing seismic event potential and adopting effective mitigation strategies. To better understand the causal mechanism of mining-induced seismicity, seismological and rock mechanics analyses need to be mutually investigated. Following Salamon (1970), many studies have shown the energy budget consideration as the missing link between seismology and rock mechanics (Garvey, 2013; Khademian & Ozbay, 2018). One approach is to use numerical modeling to analyze the state of energy of the rock during mining operations. The occurrence and intensity of a seismic event can be recognized when there is a relatively significant release of energy in the system. However, the uncertainty in the required field data to perform such analyses has limited their applicability. The question is what level of detail in the data requirement is necessary to obtain an acceptable seismic potential forecast in a longwall mine.

In 2022, the National Institute for Occupational Safety and Health (NIOSH) initiated a research project to investigate requirements for using models to estimate seismic potentials in a longwall setting. The objective is to integrate the historic seismic data and developments in the energy-balance approach for understanding mechanisms of longwall-induced seismicity and estimating the potential for destructive seismic activities. A series of tasks has been defined

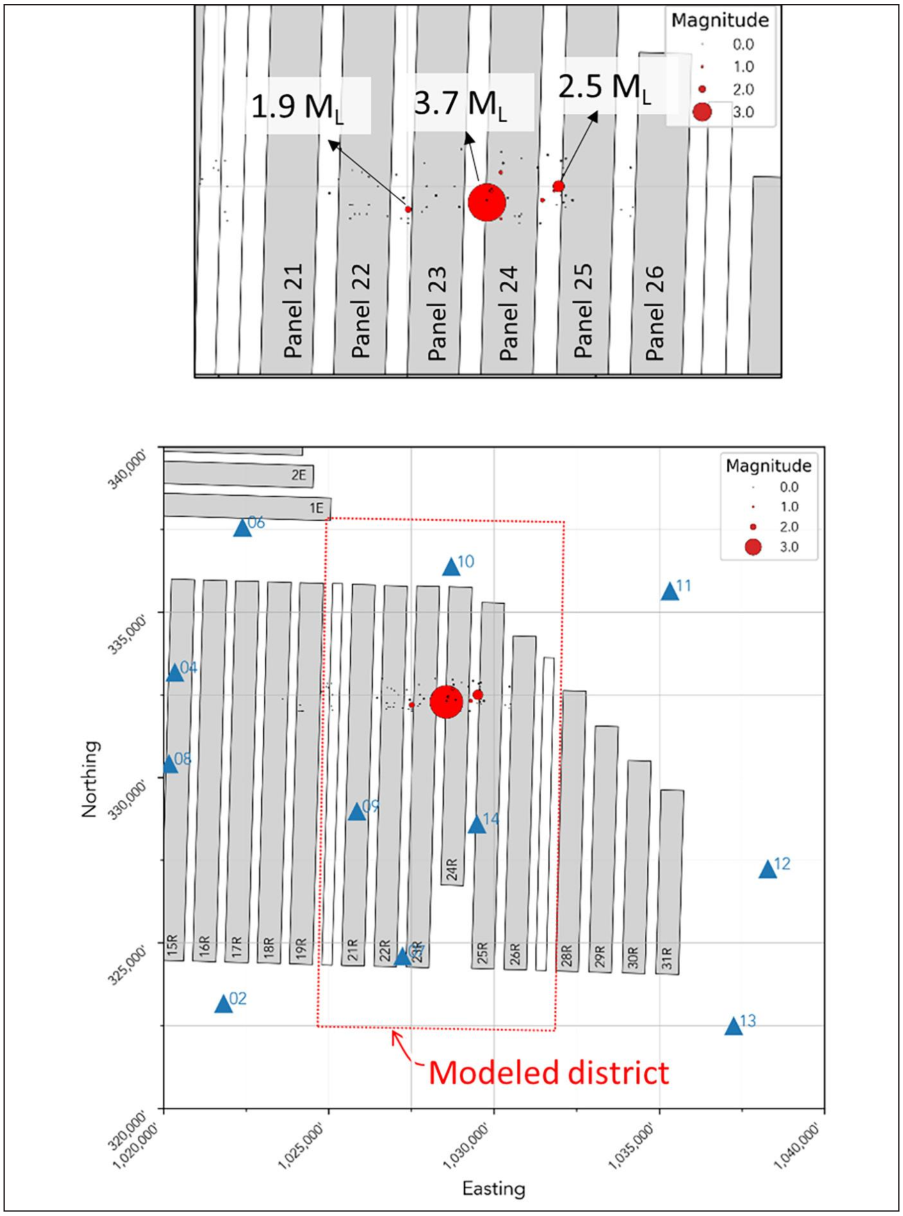

Figure 1. Plan view of panels in modeled districts along with the recorded seismic events and surface station locations

to investigate the level of complexity needed in a model for an acceptable forecast of seismic events in a longwall mine.

The seismic database in a deep longwall mine in western Virginia is used for developing and testing a methodology for forecasting seismic potential with a varied level of complexity in geomechanical data. As the first step, a pseudo-2D, three-panel, elastic model was constructed for a cross section at the location of three anomalous events that occurred in the mine in 2016 (Khademian et al., 2023). The first event occurred on June 13, 2016, with a local magnitude of 2.5 M_L. The second event happened five days later with a magnitude of 3.7 M_L followed by a 1.9-M_L event on July 20. All three events occurred during mining panel 25. From the surface seismic stations shown in Figure 1, the 2.5-M_L event occurred over the tailgate of panel 25, but the 3.7-M_L event and the 1.9-M_L event occurred over the tailgates of panels 24 and 23, respectively.

Khademian et al. (2023) developed and evaluated the seismic potential forecasting (SPF) methodology using pseudo-2D models. One model included panels 23, 24, 25 and showed that the developed methodology could have forecasted the approximate timing and location of these three events. Another model constructed previous panels 19, 21, and 22 that based on the surface seismic stations, little to no seismic activity occurred during their mining. The use of the SPF methodology showed very limited seismic potential during mining of panels 19, 21, and 22. However, the models were pseudo-2D so previous knowledge on the location of the three events along the panel was the basis of the selected cross section to be modeled.

In the next step in evaluating the SPF methodology, this paper presents the process of developing a three-dimensional model of an area including panels in the entire district. Results show that the approximate timing and location of anomalous events along the panels agree with the date and location of events recorded by the surface seismic stations. This study paves the way for the next step of the investigation which involves forecasting seismic potentials in advance of mining for districts with different mine layouts.

GEOLOGY DESCRIPTION

The longwall mine under study in this paper operates within the Pocahontas #3 coal seam in western Virginia. The Pocahontas formation that hosts the Pocahontas #3 coal seam consists of a thick lens of sediments, including cyclothem intervals of sandstone, siltstone, shale, coal, and claystone (Englund & Briggs, 1974). The mine is located within the Virginia overthrust belt. The major fault near the mine is the Keen Mountain fault that is a strike-slip fault with compressional overthrusting (Molinda, 2003). However, except for small synthetic thrust faults within the mining area (a minor offset of a maximum of 1.5 m), the Keen Mountain fault does not impact the mine.

The overall mine roof lithology consists of a sequence of shales that vary from 0–7.6 m in thickness directly above the Pocahontas #3 coal seam (Figure 2). Above the shale at the immediate roof of the mine, there is the first sandstone unit, named the Sandstone #1 (SS1), which varies in thickness from 0–10.7 m across the mine. The SS1 unit is thin to medium bedded with shale or mica streaks.

Above the SS1 unit, there is a shale parting that typically ranges from 0 to 1.5-m in thickness followed by another sandstone unit (SS2). The shale parting is present in the majority of the mining area, however, the parting is absent in some areas, composing one massive sandstone unit. The SS2 unit is generally thicker, cleaner, and a more massive sandstone compared to SS1 and can be categorized as thickly to massively bedded. The SS2 unit generally varies from 9.1 to 22.8-m in thickness.

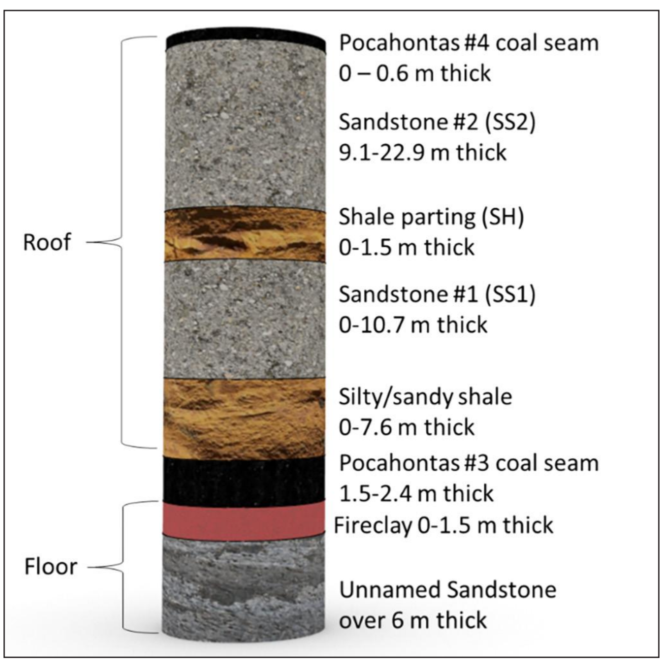

Figure 2. Generalized stratigraphic column of the mine area

SEISMIC HISTORY

Seismic activity related to the longwall mine has shown similar tendencies across the several districts that have been seismically monitored. Generally, the events can be grouped into those that are very near, spatially and temporally, to the longwall mining face, which tend to be of small magnitude, and those that vary greatly in magnitude and can continue to occur for many months after longwall mining has ceased in a district. The events in the district generally show the typical preference for the tailgates of panels, although there is variability in distribution from location to location within the district. There does not appear to have been a preference of higher magnitudes to have been located toward the tailgate, relative to the lower magnitudes—the distribution of higher magnitudes is similar to that of lower magnitudes. However, there is a scatter in the generated event locations, which is certainly due to location error.

The event location error is impacted by factors, such as the picking error of wave arrival time and velocity model inaccuracy. The uncertainty in event location is significantly larger for events located with automatically generated arrival times versus manually generated (human inspected) arrival times, and this effect is inversely correlated with magnitude as smaller events will have smaller signal levels relative to background. The horizontal uncertainties for events located by manual picks are generally confined to a few tens of meters, while those for events located by automatic picks can vary greatly, with larger events constrained to within a few tens of meters, but smaller events sometimes being constrained to within a few hundred meters, and occasionally more. The vertical component of the event locations here is underconstrained, and errors routinely exceed hundreds of meters, depending mostly on horizontal distance to nearest recording station.

The vast majority of the seismic events at the mine exhibit dilatational first motions at all surface recording stations, suggesting a large isotropic component, consistent with a downward displacement of rock mass. Some events, particularly within the set of events larger than 1 M_L, exhibit a small compressional first motion within a range of azimuths, suggesting a small slip on a plane of failure associated with the event, and occurring at its initiation time. This non-isotropic contribution to the energy release varies in size for different events but is typically small compared to the overall size of the event. The 2.5-M_L and 3.7-M_L events which occurred in July 2016 in close proximity to each other both exhibited a small amount of compressional first motion at two recording stations located to the south of the events (Khademian et al., 2023). Note that while dilatational first motions are certainly suggestive of implosive events, and that is an acceptable way to get an initial idea of an event's mechanism, first motions alone are not sufficient to determine event source mechanism. There can be more complex mechanisms that have a combination of shear and implosive components that still have all dilatational first motions. There could also be poor sampling of the focal sphere depending on where the event locates within the network. A detailed focal mechanism study is planned for future work to gain more certainty on the source mechanism of the events.

GEOMECHANICAL MODEL

For replicating the geologic variability across the district, a MineScape geology model (Datamine, 2021)(Datamine, 2021) developed by the mine was used. The modeled geology was consistent with the lithology found in the nearby core holes. The surface maps of the bottom of coal, top of coal, top of immediate roof shale, top of SS1, top of shale parting, and the top of SS2 were extracted from the MineScape geology model and converted into interfaces in a 3DEC model (Itasca, 2016). A 3D elastic model in 3DEC was constructed to cover the entire district containing six panels as shown in Figure 3.

Figure 3 shows the overall model geometry with a zoomed-in view of panels 24 and 25 at the cross section (Figure 1) where the three anomalous events occurred. As shown in Figure 3, the thickness variation of each lithology was modeled so that the absence and presence of the parting shale and immediate roof shale was captured across the model.

The geomechanical properties used in the model are listed in Table 1. The bedding plane cohesion was kept high intentionally to avoid bedding plane sliding for later calculating slip-type seismic potential. The tensile strength of the contacts was, however, kept at an average value of 0.5 MPa to allow bedding separation. The friction between sandstone units was 30 degrees and 20 degrees for shale-sandstone interfaces. For coal interfaces in the roof and floor, the friction was assumed to be 10 degrees. Note that the goal of this stage of research was to understand if a simplified elastic model with no account for inelastic deformation, gob formation, and bedding plane sliding can provide useful information for seismic potential forecasting.

In-situ stress

The horizontal stress gradients are obtained based on the local stress measurements and modification to the Mark and Gadde (2008) stress equations for the Eastern mine. Table 2 lists the results of overcoring stress measurement at different locations in the mine.
Figure 4 shows the maximum horizontal stress magnitudes on a plot

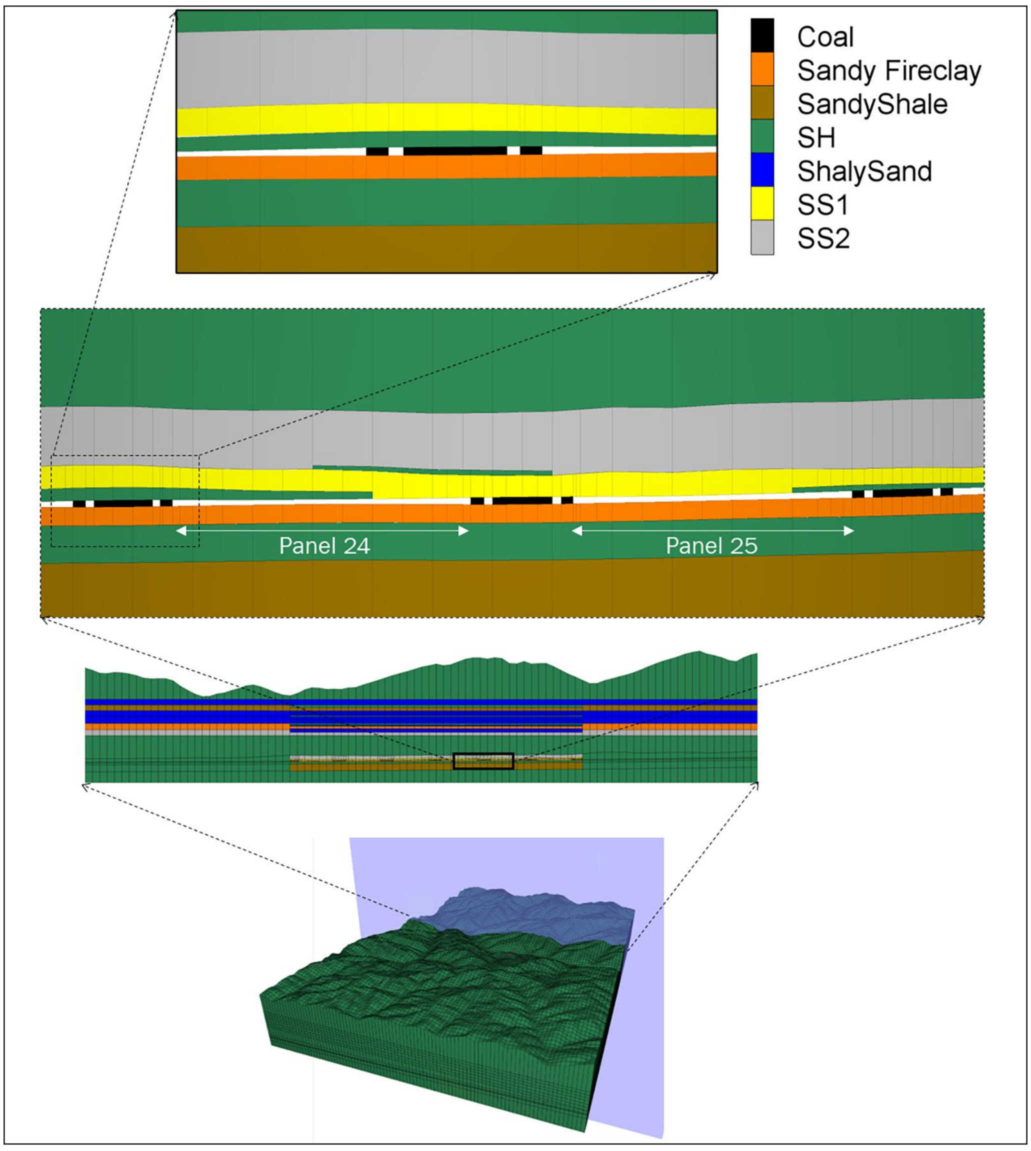

Figure 3. Three-dimensional geomechanical model in 3DEC with roof strata variation in thickness

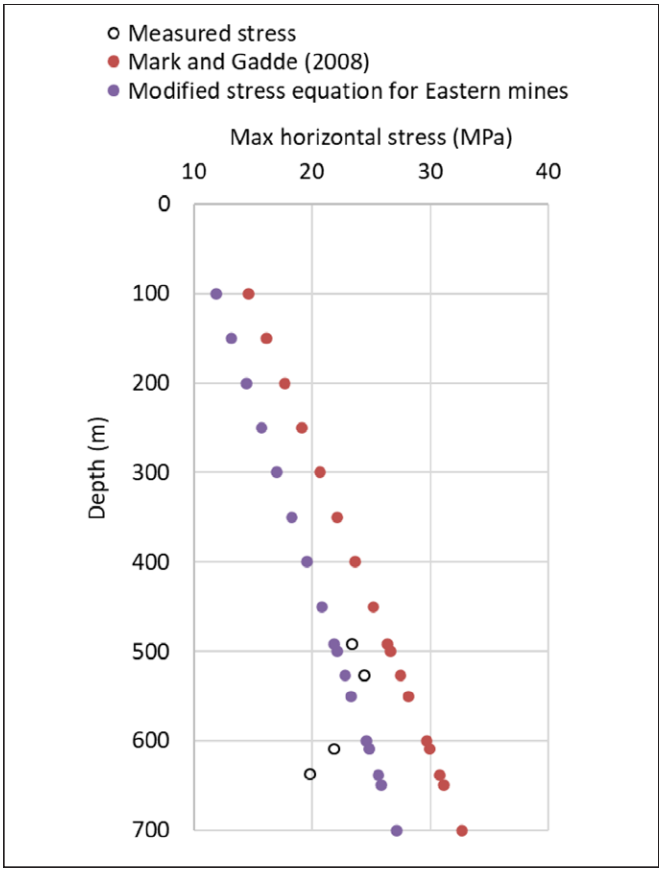

Figure 4. Average stress gradient from the stress measurement results

Table 1. Geomechanical properties used in the 3DEC elastic model. UCS values were used for later calculation of compressive-type seismic potential.

Rock Type	Young's Modulus (GPa)	Poisson Ratio	UCS (MPa)
Coal	1.7	0.35	7
Sandy Fireclay	22	0.25	60
Shaly Sand	20.9	0.2	60
Sandy Shale	16	0.26	40
Shale	10.3	0.26	33
SS1	22.9	0.2	68
SS2	28.4	0.2	90

with the Mark-Gadde stress prediction equation with an average 30-GPa elastic modulus along with the measured stress points from Table 2. A revisit at pre-mining horizontal stress in coal mines based on Mark and Gadde (2008) and Dolinar (2004) data was performed, and a modified equation was used to represent the gradient of the maximum horizontal stress in the model as shown in Figure 4. This process is explained below.

Mark and Gadde (2008) used overcore stress measurement data in U.S. coal mines and coal measure rocks to predict the field stress in coal mines. They developed an equation for the maximum horizontal stress in MPa of the form:

$$S_H = a + (b \times D) + (c \times E) \tag{1}$$

where *a*, *b*, and *c* are constants determined through regression analysis of field measurements. *D* is depth of cover in m and *E* is elastic modulus in GPa. The *b* parameter might be considered to be the Poisson effect and the *c* parameter the tectonic strain effect. Mark and Gadde (2008) developed an equation for eastern mines, including the Illinois basin and one for western mines, (Colorado, Utah). The *a*, *b*, and *c* parameters for the eastern mines were calculated to be 2.6 (MPa), 0.03 (MPa/m) and 0.3, respectively (Mark and Gadde 2008). However, Dolinar (2004) showed that for the eastern U.S., the scatter of data can be reduced by considering it as two sets—low and high tectonic strain regions. The high tectonic strain region is associated with mines in southern West Virginia, mainly associated with the Beckley seam. Figure 5 shows datapoints of the maximum horizontal stress measurements plotted versus depth and elastic modulus of the rock layer tested (Mark and Gadde, 2008).

The diamonds in Figure 5 show the stress values in an abnormally high stress region within the Beckley area in southern West Virginia. Each datapoint is color coded to show they can be considered outliers in either elastic modulus or depth plots. The same color diamond shows the same stress point in both plots. If the abnormally high stress associated with the Beckley area in southern West Virginia are treated as a separate group, the eastern U.S. data can be presented by the following two equations (stress in MPa, depth in meters and modulus in GPa):

$$tS_H = 0.346 + (0.025 \times D) + (0.301 \times E) \tag{2}$$

For mines in the high-strain area of southern West Virginia, the following equation can be used:

$$S_H = 8.7 + (0.041 \times D) + (0.192 \times E) \tag{3}$$

Figure 6 is a type of "residual plot" that helps evaluate the performance of the regression in Equation 2. Figure 6(a) and Figure 6(b)

Table 2. Horizontal stress measurement results in the mine

Test Locations	Max Horizontal Stress (MPa)	Min Horizontal Stress (MPa)	Max Horizontal Stress Orientation	Overburden Stress (MPa)
1	23.4	11.3	N71.2E	12.6
2	24.5	11.4	N66.1E	13.4
3	21.9	15.4	N58.1E	15.6
4	19.8	10.9	N67.1E	16.3

compare the maximum horizontal coal mine stresses predicted by Equation 1 and Equation 2, respectively, against the measured values for the mines in the eastern U.S. The filled circles in Figure 6a show the regions with abnormally high horizontal stress detected in Figure 5. The R-squared for the regression of Equation 1 is 0.5 but is improved to 0.8 in Equation 2 after removing the high-stress regions in the Beckley area.

From the overcoring stress measurements in Table 2, the minimum horizontal stress to maximum horizontal stress ratio ranges from 0.5 to 0.7 with an average of 0.6. The in-situ stress was applied to each layer in the model based on their depth and elastic modulus following Equation 2.

Mining Sequence

In the district under focus, the overburden depth ranges from 400 to 650 m. The panels were 304-m wide with a 4-entry system of pillars. The panels were approximately 3500-m long except for panel 24 with a length of 2700 m. A large area of the 24 panel longwall pillars was identified as a hazardous area for seismic potential based on geological criteria defined by mine geologists and NIOSH researchers (Van Dyke et al., 2023). Therefore, the

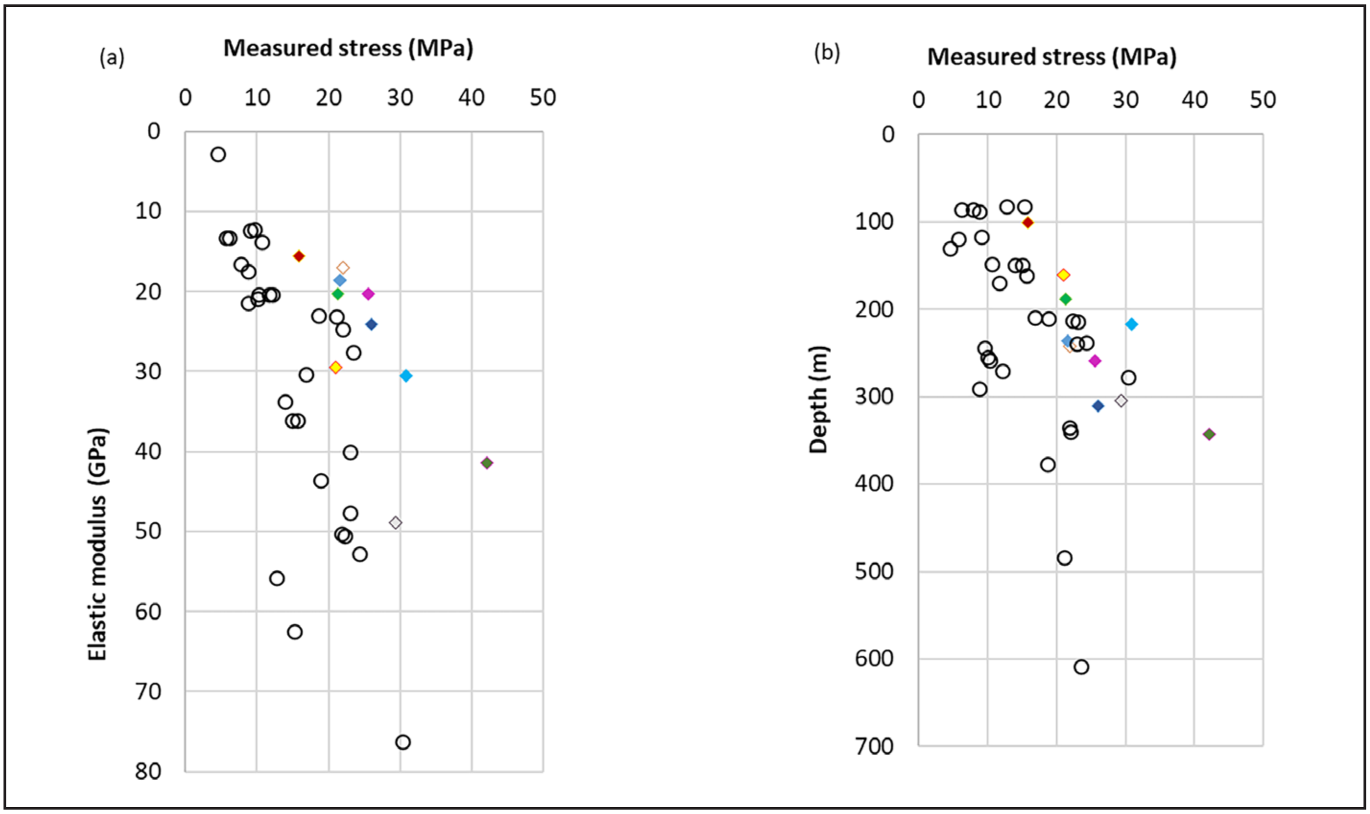

Figure 5. Stress measurement database in the Eastern U.S. coal versus (a) elastic modulus and (b) depth (after Mark and Gadde, 2008)

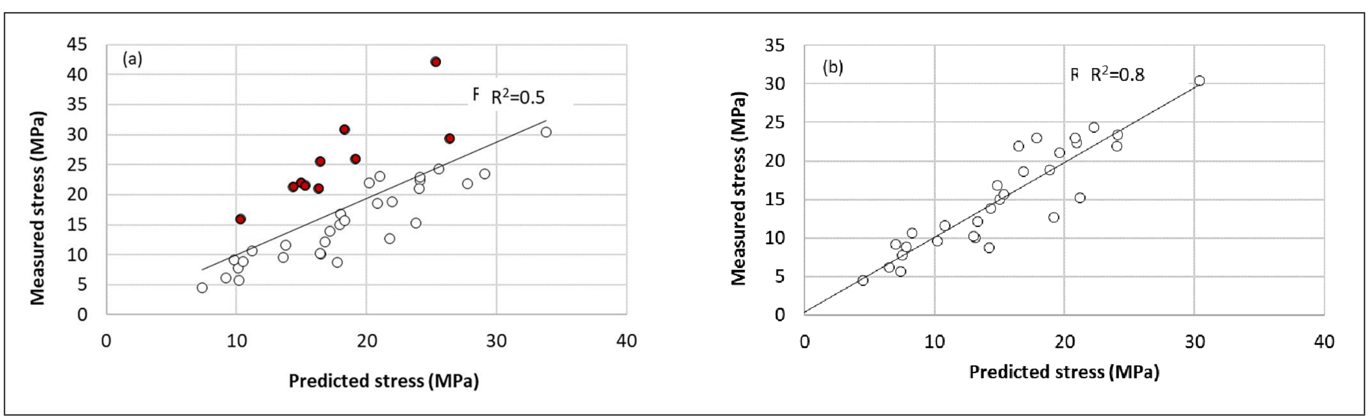

Figure 6. Overcoring stress measurements versus predicted stress before (a) and after (b) excluding abnormally high-stress regions in West Virginia

decision was made by mine management to move the longwall setup face approximately 760 m north of the intended mine plan.

Figure 7 shows the overall geometry of the model and the panel layout. After applying in-situ stress to each layer in the model based on their depth and elastic modulus, the model was brought to equilibrium. Then, all development works were mined followed by mining the panels according to the operational schedule and mining sequence.

The mining process was not explicitly simulated and thus each panel was mined by removal of coal within the panel with no consideration for gradual relaxation of the roof and floor because the model materials are assigned elastic. The subsidence profile after completing the last panel is shown in Figure 7 with the maximum subsidence of 0.35 m (1.14 ft) occurring above panels 23 and 24 when the last panel was mined. Note that the mining height on average is 1.8 m (6 ft).

SEISMIC POTENTIAL FORECASTING (SPF) METHODOLOGY

For studying mining-induced seismic events, energy balance equations are a possible link amongst rock failure mechanics, main geology features, and seismology. When mining underground, at each stage of development, energy becomes available from the work (W) done by external forces that causes the convergence of the opening and the strain energy that is stored in the mined-out area U_m During mining, some of this available energy is consumed (W_p) through inelastic deformations such as panel roof caving and pillar yielding, and some of it is stored as strain energy (U_c) in competent rock strata. If this available energy ($W + U_m$) exceeds the sum of consumed energy and stored energy, seismic energy (W_k) can be radiated during the rock failure process, leading to instability. The following equation represents energy budget changes by the mining process (Salamon, 1970).

$$W + U_m = W_p + U_c + W_k \quad (4)$$

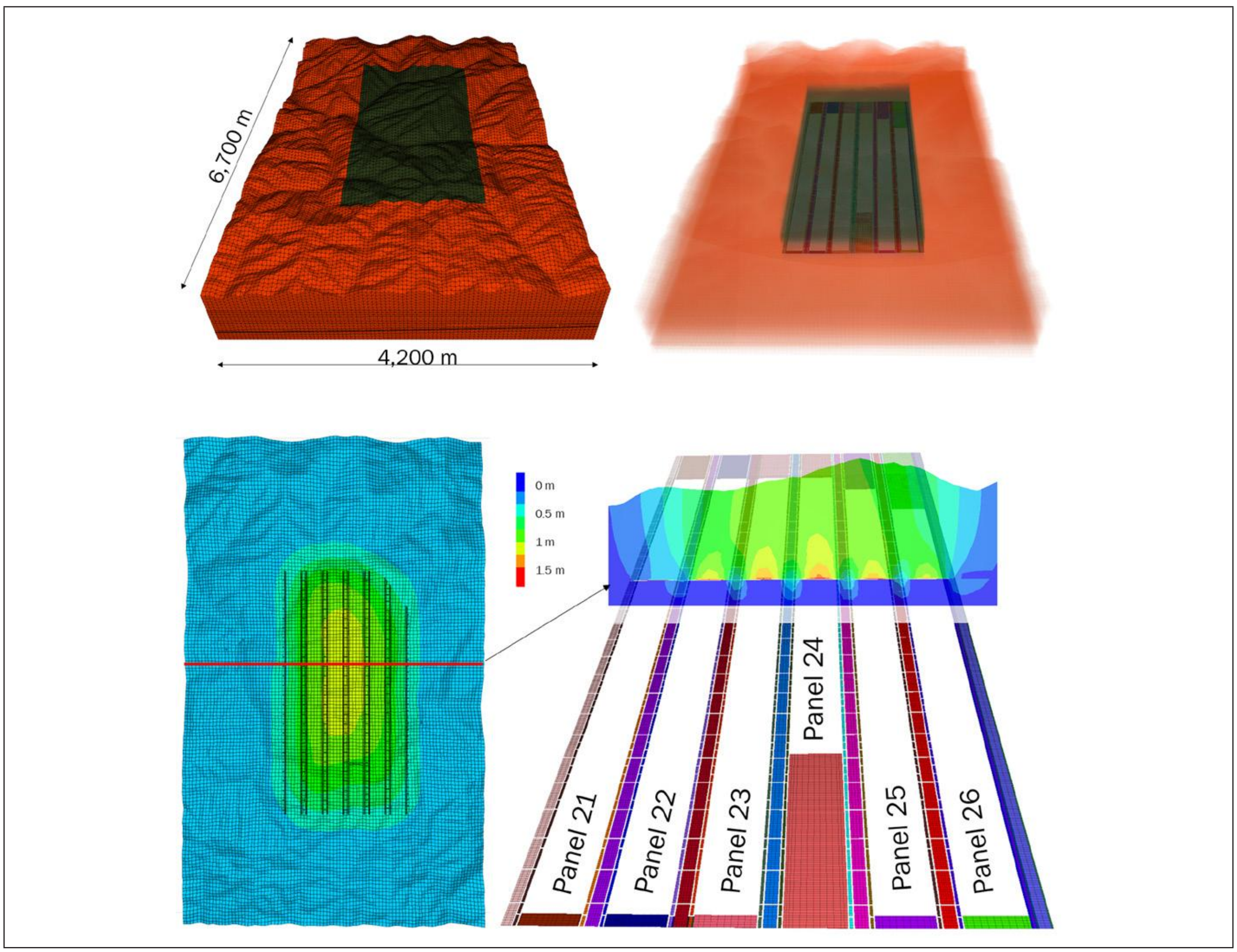

Figure 7. Modeling results after completing all panels in the district following the actual mining sequence

Seismic events can be the result of a sudden release of compressive stress through crushing of the rock with a dilatation signal or a sudden release of shear stress through slip along discontinuities or intact rock with a standard 4-quadrant fault plane signature.

Many studies investigated the release of energy and potential for seismic activities through fully solving the energy balance at each stage of mining and calculating W_k. (Garvey, 2013; Khademian & Ozbay, 2018). However, such an approach requires the calculation of W_p that needs complex constitutive models to simulate strain-weakening rock failure and slip-weakening sliding through pre-existing discontinuities and main geologic features. The main uncertainty in such a modeling exercise is the weakening response (post-failure) of the rockmass and discontinuities under mining-induced stress. In order to provide a benchmark for such complex mechanical models, this paper makes simplifying assumptions and uses indirect indicators of W_k to assess seismic potentials in a mining setup. However, extensive rock mechanics tests have recently been conducted to quantify the post-failure response of different rock types in the study mine and will be used for the next step of this research for fully solving the energy balance equations.

In an elastic model, two main questions need to be addressed for seismic potential analyses. The first question is how to detect the occurrence of an event in an elastic model. The second question is how to estimate the intensity of seismic events in an elastic model. In an inelastic model, the occurrence of a seismic event depends on the stress level, post-peak response of rock, interface rate- and slip-dependent frictional properties, and loading system stiffnesses. Probably a simple yet practical indication of occurrence of failure in an elastic system is the level of stress compared to the rock strength. As for the intensity of an event, studies showed that the initial state of strain energy and its variation with mining can be an indicator of seismic event intensity (Mitri, Tang, Comeau, & Mohammed, 1999). In other words, once conditions for seismic failure are met, the higher budget of energy available in the system ($W + U_m$) may lead to the higher level of W_k. Assuming rock is perfectly elastic and mining advances gradually, energy available in the system is fully stored as U_c in Equation 4, and thus in an elastic system U_c is a measure of the available energy.

Compressive-Type Events

Castro, Bewick, & Carter (2012) and Martin, Kaiser, & Mccreath (1999) proposed a deviatoric stress approach to identify zones with the potential for rock mass damage initiation around a deep opening, given as:

$$(\sigma_1 - \sigma_3) = 0.4 \text{ to } 0.5 \ \text{UCS} \tag{5}$$

Castro et al. (2012) defined a ratio of 0.6 UCS to 0.7 UCS for moderate potential and > 0.7 UCS for major potential of seismic events. In this paper, zones prone to high-energy events, referred to as seismogenic zones, were identified if they satisfied inequality (6) below:

$$\frac{(\sigma_1 - \sigma_3)}{\text{UCS}} > 0.7 \tag{6}$$

Then, U_c stored strain energy was calculated within the seismogenic zone as the difference between the initial (pre-mining) and current state of Strain Energy given as:

$$\textit{Strain Energy} = \sum \frac{V}{2E}\begin{bmatrix} \sigma_1^2 + \sigma_2^2 + \sigma_3^2 \\ -2\Omega(\sigma_1\sigma_2 + \sigma_1\sigma_3 + \sigma_2\sigma_3) \end{bmatrix} \tag{7}$$

where σ_1, σ_2, and σ_3 are the principal stresses in each zone in the model; ν and E are the Poisson ratio and Young's modulus of the rock. V is the volume of each zone.

Slip-Type Events

During mining activities, the occurrence of shear-type seismic events induced by mining are frequently reported ranging from pure shear-type moment tensors to a combination of shear and compressive-type events (Ryder, 1988). For the slip-type events, W_p in Equation 4 is the result of frictional sliding along discontinuities. Initiation and propagation of rupture depends on the stress level, slip- and rate-weakening friction properties, and the loading system stiffnesses (Khademian & Ozbay, 2018). However, as a simplified indicator for the seismic potential of a discontinuity, Ryder (1988) defined Excess Shear Stress (ESS):

ESS=Prevailing shear stress prior to slip –dynamic shear strength

ESS follows the logic that the prevailing shear stress on the fault is an important factor because W_k (Equation 4) cannot emerge if the level of stress is lower than the dynamic strength of the fault. Figure 8 explains the ESS concept. The red line is the shear stress on a discontinuity that meets with the static friction curves at a few points that could be the rupture initiation point. Once activated, the strength of the discontinuity drops to the dynamic friction leading to a rupture. In short, ESS can be viewed as the net force available to drive a slip-type seismic event.

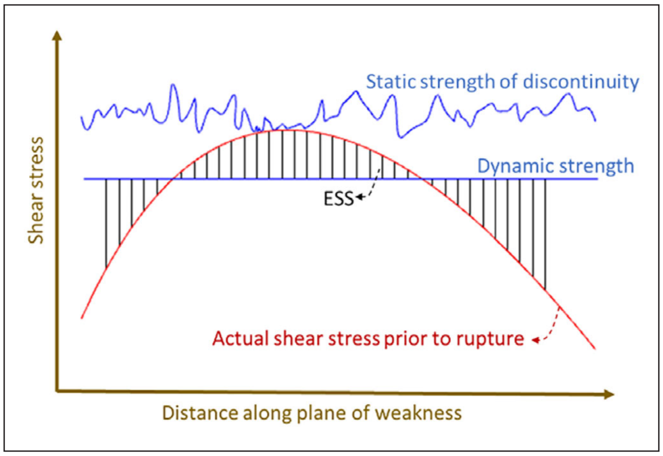

Figure 8. Shear stress and strength conditions along a plane of weakness (After Ryder, 1988)

Careful laboratory experiments and field calibration are needed to define the range of ESS that can lead to high seismic potentials, but in the meantime, the following suggested representative values (Ryder, 1988) are used in this paper:

ESS <0: No event is possible.
ESS <5 MPa: slip-type seismic activity is unlikely.
ESS >15 MPa: Anomalous slip-type seismic events are likely.

The average ESS is calculated along each bedding plane in the model. Each contact element with ESS>5 MPa is referred to as seismogenic contact or interface. For estimating the intensity of a slip-type seismic event, it is assumed that ESS is distributed evenly over the seismogenic interface. From Ryder (1988), for a uniformly distributed ESS, seismic moment can be calculated from:

$$M_o = 2.25\ \tau_e\ A \tag{8}$$

where τ_e is the ESS average over the seismogenic plane with area A. W_k can then be estimated from:

$$W_k = \frac{M_o \tau_e}{2G} \tag{9}$$

where G is the shear modulus of the surrounding rock and can be the average of the two strata comprising the interface. Table 3 lists a summary of the criteria for identifying a seismic event and estimating its intensity in a simple elastic model.

Table 3. Criteria for identifying the occurrence and intensity of seismic events in elastic media

Event type	Shear	Compressive
Event occurrence criteria	ESS > 5 MPa	$\frac{(\sigma_1 - \sigma_3)}{UCS} > 0.7$
Event intensity upon occurrence	W_k in Eq. 11	U_c in Eq. 7

Implementation

The methodologies explained above are implemented in the 3DEC geomechanical model for forecasting seismic event potential. To this purpose, first the slip-type and compressive-type events were detected during mining each panel following the occurrence criteria in Table 3. Then, the intensity of the events was forecasted based on the energy criteria in Table 3. For visualization, the entire model was discretized into vertical square prisms. W_k and U_c energy terms in all the zones that fell within each of the prisms were separately summed and saved as attributes of the prism. The maximum W_k and U_c values at the end of completing the last panel were used to normalize the W_k and U_c energy terms in each prism. The maximum W_k was 2.4 GJ and maximum U_c was 1 GJ. Then, two heat maps were developed to show the seismic potential associated with slip-type and compressive type events. In each heat map, each prism was shown as a square whose color represents the intensity of the normalized W_k or U_c energy terms. Each square in the heat maps represents the entire vertical column of zones in the model at that location. The color bar is arbitrarily divided into 13 seismic potential indices with increasing seismic potential from 1 to 13 and from cool to warm colors. This process is repeated after completing each panel in the district.

RESULTS

A series of heatmaps was developed for slip-type and compressive-type events after the completion of each panel in the district. The mine layout and recorded seismic events by the surface stations were drawn on each map, following the mine sequence. For example, when panel 24 was mined in the model, the seismic events recorded before the completion date of panel 24 were superimposed on the seismic potential maps. Two ranges of events in terms of magnitude were superimposed on each map, one for events with magnitudes above zero M_L and one for events of magnitudes above 1 M_L. This paper presents and discusses the heatmaps after mining panel 24 and panel 25.

Compressive-Type Events

Figure 9 shows the seismic potential forecasting maps related to compressive-type events after mining panel 24. From mining previous panels, elevated-potential areas were forecasted in the headgate of panels 21 and 22 with a maximum C-SPI of 13 at location (300, 800). The corresponding recorded events in that area show 38 events <1 M_L and one event of magnitude 1.1 M_L but no event above 2 M_L. That means the map forecasted a false positive event that will be discussed later in this paper.

The pattern of the elevated seismic potential changed when the next panel, panel 25, was mined as shown in Figure 10. The model forecasted an elevated seismic potential in the tailgate of panel 24 at location (950, 2500) with SPI of 13 (corresponding to the timing and location of a 3.7-M_L event recorded by surface stations) and an elevated zone in the headgate of panel 24 with SPI 9 at (1,200, 2,500) and (1,200, 3,000) that correspond to a 2.5-M_L event in terms of timing and location.

To investigate the performance of the seismic forecasting maps, a concept of confusion matrix was used. A confusion matrix explains how many of the actual events were correctly classified by the forecasting map. For constructing the confusion matrix, the seismic potentials based on recorded events were grouped as *actual* potential with subgroups that were based on the following descriptions:

- Zones (squares in the heatmaps) in the model that included seismic events below 1 M_L within a 90-m radius from the zone centroid were grouped as *actual* "low" potential.
- Zones that included seismic events below 2 M_L within a 90-m radius from the zone centroid were grouped as *actual* "moderate" potential.
- Zones that included seismic events above 3 M_L within a 90-m radius from the zone centroid were grouped as *actual* "elevated" potential.

For forecasted seismic potential, zones in the map were grouped as *forecasted* potential with subgroups based on the following description:

- Zones (squares in the heatmaps) with SPI below 5 were considered *forecasted* "low" potential.
- Zones with SPI below 10 were considered *forecasted* "moderate" potential.
- Zones with SPI above 10 were considered *forecasted* "elevated" potential.

The 90-m radius for the buffer zone is based on the discussion in Section 3 and followed previous works (Van Dyke et al., 2023). Figure 11 shows the confusion matrix for the forecasted C-SPI. The diagonal terms in a confusion matrix show the successful forecast of actual events. The non-diagonal terms show false positive and false negative forecasts. As shown in Figure 11, 100% of elevated-potential and moderate-potential regions, and 88.8% of low-potential zones were forecasted correctly. There were no false negative forecasts, but 0.2% and 11% of *actual* low-potential zones were forecasted to be elevated and

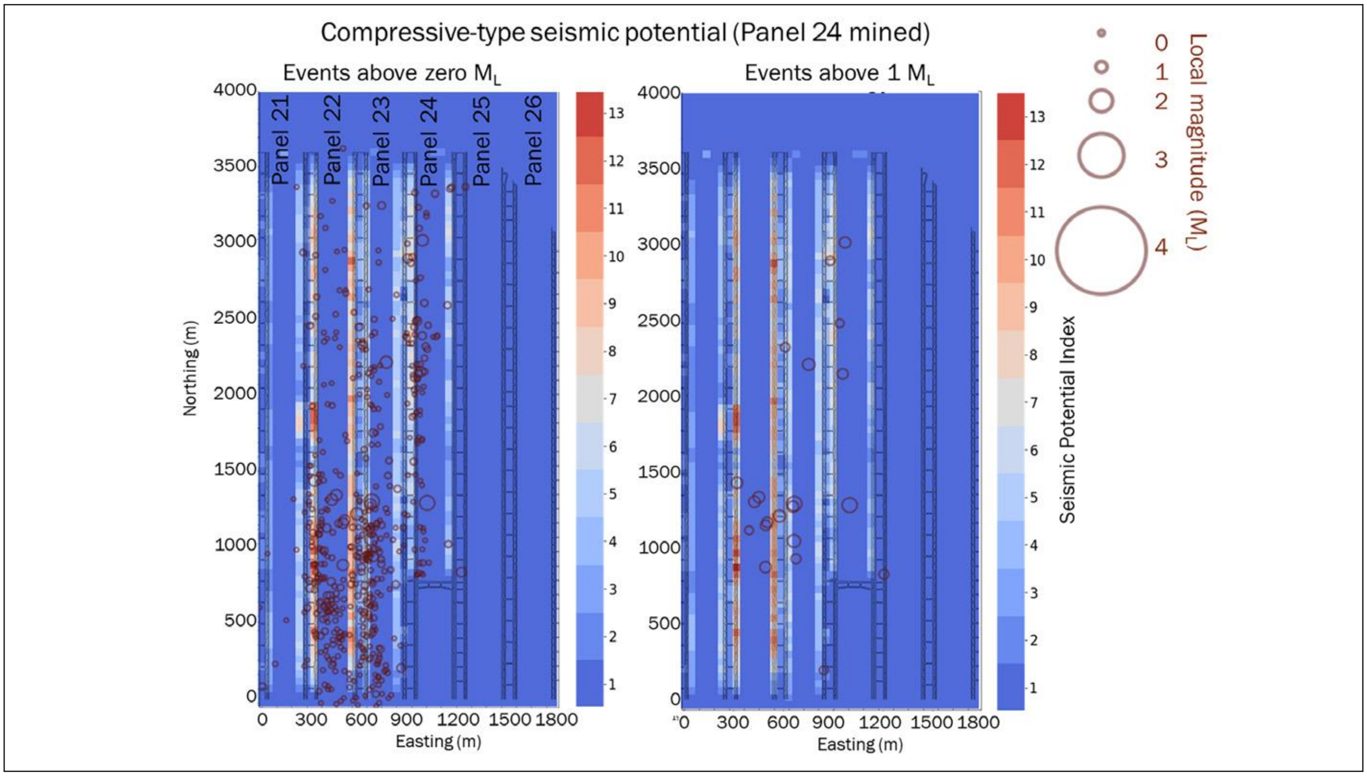

Figure 9. Seismic potential forecasting map for the compressive-type events after completing panel 24. The mine layout and recorded seismic events are also shown for clarification.

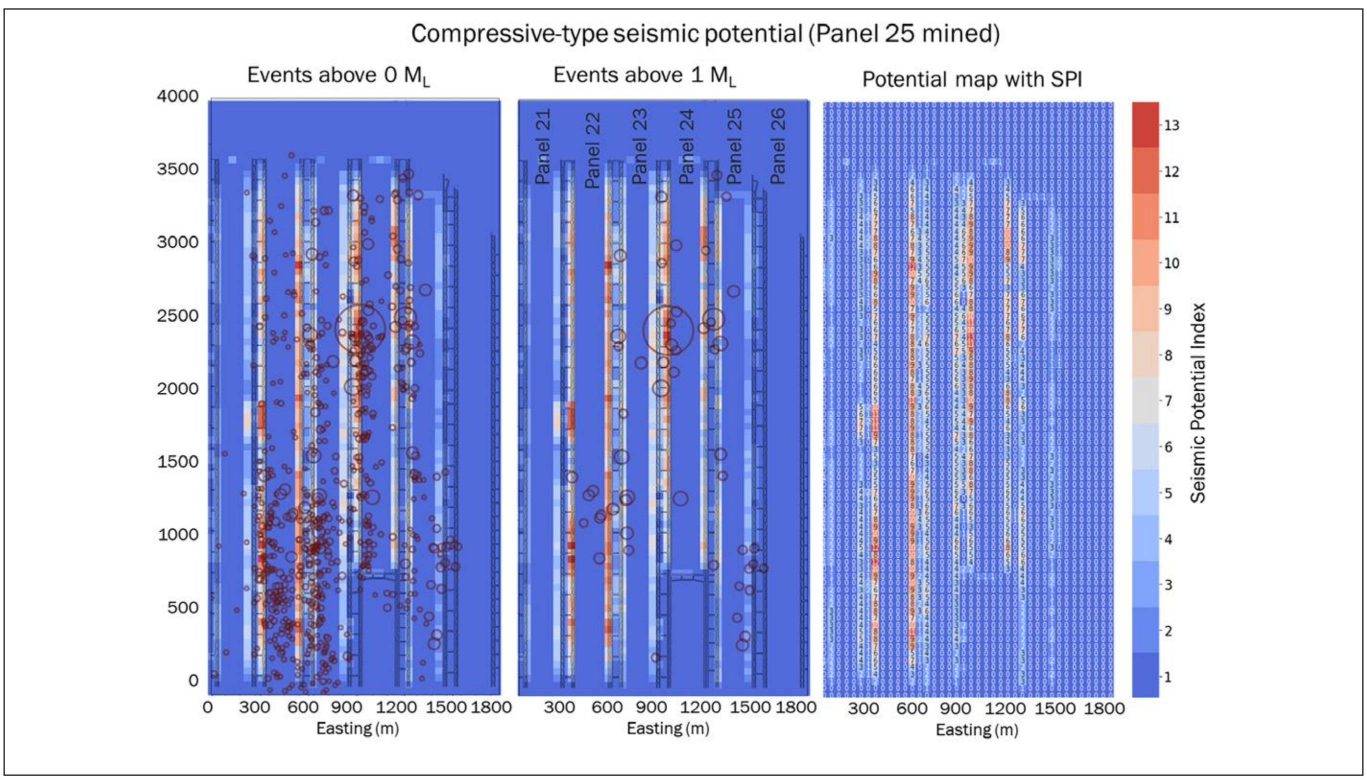

Figure 10. Seismic potential forecasting map for the compressive-type events after completing panel 25. The mine layout and recorded seismic events after mining panel 25 are also shown for clarification.

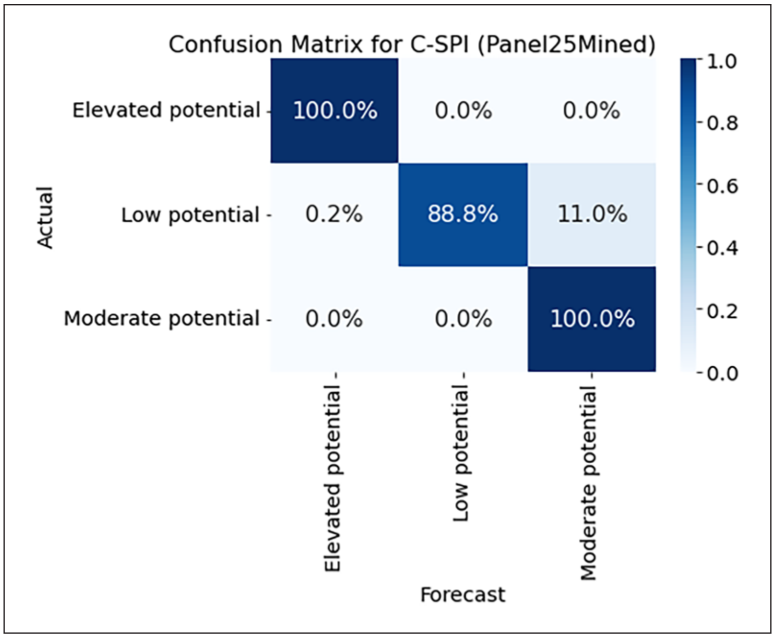

Figure 11. Confusion matrix for the seismic potential map for the compressive-type event. Two non-diagonal cells are non-zero, showing false positive forecasts. 0.2% of low potential events are forecasted to be "elevated" and 11% of low potential events are forecasted to be "moderate."

moderate-potential zones, respectively, which are false positive forecasts. This misclassification is related to the high C-SPI values at (300, 800), (300, 900), and (600, 2700) that do not correspond to zones of *actual* elevated potential. For example, as shown in Figure 10, the headgate of panel 21 (300, 800) shows a SPI above 10, while no corresponding anomalous events of magnitude above 2 M_L occurred within a 90-m radius of that location. Instead, the surface seismic stations recorded the occurrence of several events of magnitudes below 1 M_L within a radius of 90 m around location (300, 800). In other words, the map is forecasting a false positive for an anomalous seismic event while the energy built-up forecasted in the model is in reality released through the occurrence of 44 events with magnitudes below 1 M_L. We try to address this issue by looking at the seismic potential for slip-type events in the next section.

Slip-Type Events

From Section 3 based on the seismic event waveforms discussed in previous works (Khademian et al., 2023), some events, particularly within the set of events larger than 1 M_L, indicated a small slip on a plane of failure associated with the event, and occurring at its initiation time. That is, for large events recorded by the surface stations, mechanisms for both slip-type and compressive-type events probably played a role in initiation and intensity of events. To this end, heatmaps were developed following the methodology explained in Section 5 for slip-type seismic potentials. As shown in Figure 12, after mining panel 24, regions around the headgate of panel 23 and tailgate of panel 24 were forecasted as moderate potential with S-SPI of 8–10 at locations (900, 500), (900, 800), (900, 2,500), and (900, 3,000). Figure 13 shows the seismic potential map when panel 25 was mined. The location of regions around the headgate of panel 23 and tailgate of panel 24 stayed the same, but their S-SPIs increased to 13, which indicates elevated seismic potential. In addition, the S-SPI in the headgate of panel 24 increased to values above 9 with the highest of 10 around the location of the 2.5-M_L event.

The location of the 3.7-M_L is also forecasted by the map with the indicator of S-SPI 13. However, that is not the only region with S-SPI of 13. The map also forecasts elevated potential with S-SPI 13 at locations (900, 500), (900, 800), and (900, 3,000). That is, there are false positive results in the calculations of the seismic potential when only considering slip-type events.

Further investigation showed that the regions that show elevated seismic potentials in slip- and compressive-type events overlap in certain locations. This means from maps in Figure 10 and Figure 13, that is evident that in the regions where both slip-type and compressive-type events have elevated SPI, anomalous seismic events were recorded by the surface station. Therefore, SPI should represent both event types for reducing false positive forecasting results. The next section attempts to combine SPI of the slip- and compressive-type events for enhancing the performance of the seismic potential forecasting maps.

Combined Seismic Potential Index

One of the hypotheses of this research is that the trigger for anomalous events is unstable sliding along bedding planes followed by the release energy in the form of stored strain energy. The results in Figure 10 and Figure 13 showed that location and timing of anomalous events can be realized where SPI of both slip-type and compressive-type events are above 10. To this end, an algorithm is developed to search through all zones in both compressive-type and shear-type potential maps to correct the C-SPI for the S-SPI. The search is first done for the C-SPI in each zone. For C-SPI above 10, if there is not a corresponding S-SPI above 10 within a 90-m

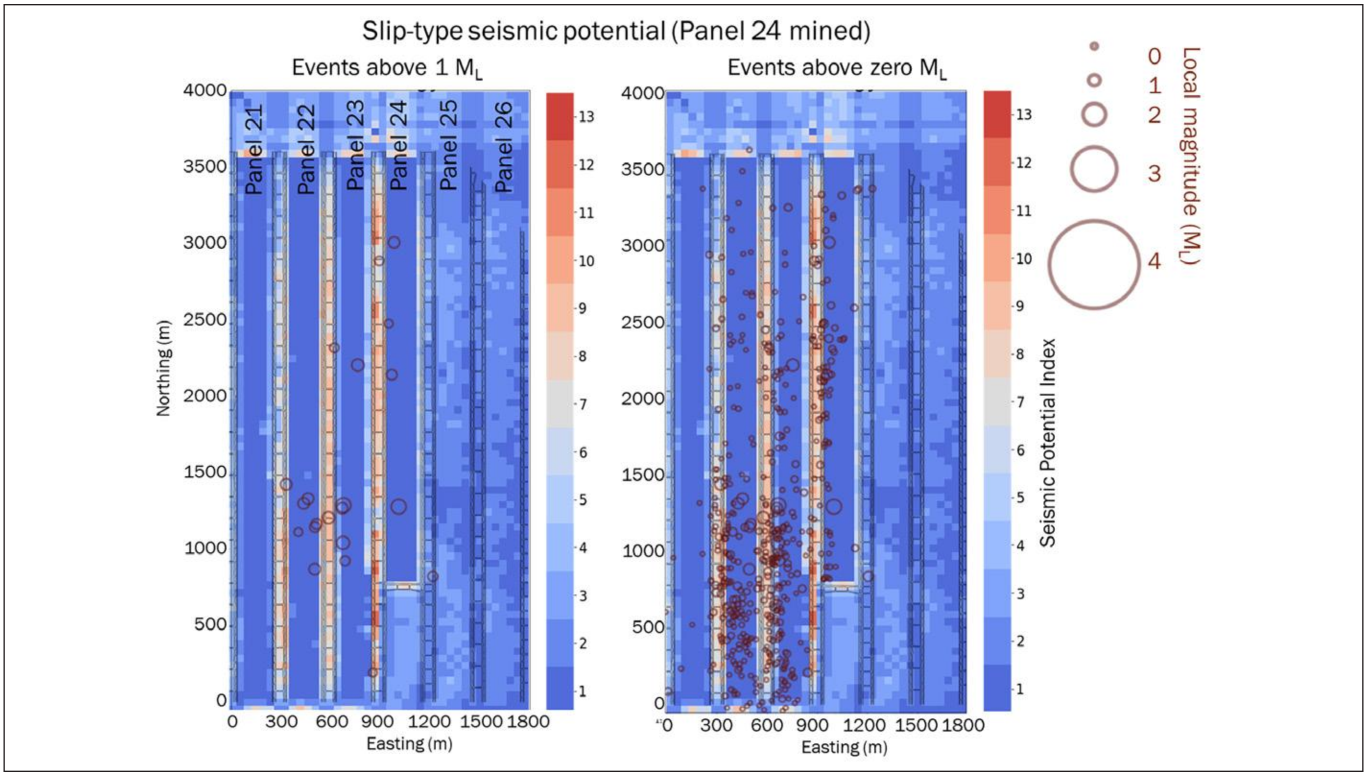

Figure 12. Seismic potential forecasting map for the slip-type events after completing panel 24. The mine layout and recorded seismic events after mining panel 24 are also shown for clarification.

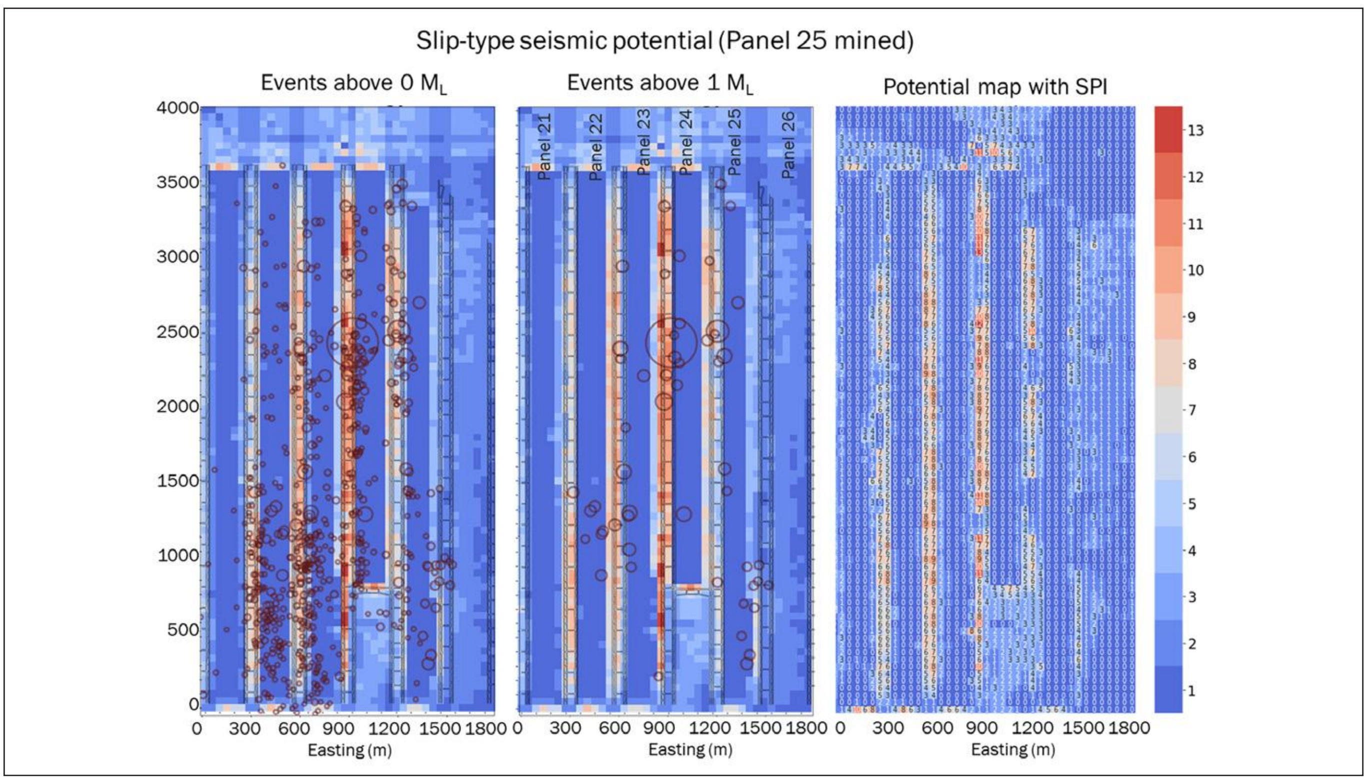

Figure 13. Seismic potential forecasting map for the slip-type events after completing panel 25. The mine layout and recorded seismic events after mining panel 25 are also shown for clarification.

radius, S-SPI is replaced with the C-SPI. The results are shown in Figure 14. In Figure 14a and Figure 14b, the corrected SPI for all regions after completing panel 25 is demonstrated. Figure 14c shows the seismic potential map with the SPI annotated in each block.

Figure 15 shows the confusion table after correcting C-SPI for S-SPI. The false positive forecasts for elevated potentials are reduced to zero. The only non-zero, non-diagonal term is 11% of the actually low potential zones that are identified as moderate events. In terms of hazard recognition, misclassifying low-potential zones with moderate-potential zones is less concerning, but further investigation will be conducted in more complex geomechanical models to remove the false positive forecasts in this group.

DISCUSSION AND LIMITATIONS

The analyses of shear stress along bedding planes through the ESS calculation and failure envelope of strata (Equation 5) in a longwall mine allowed for the calculation of an index for forecasting seismic

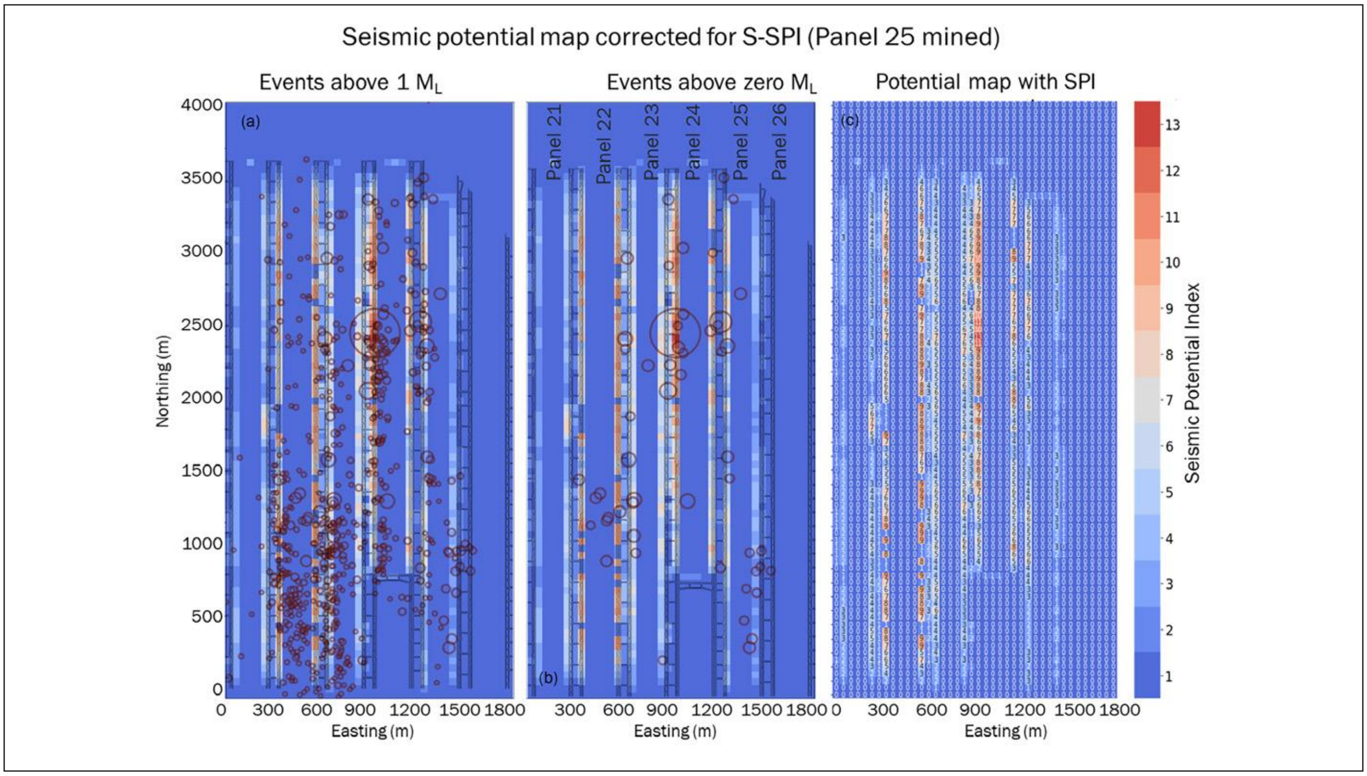

Figure 14. Combined seismic potential indices after mining panel 25

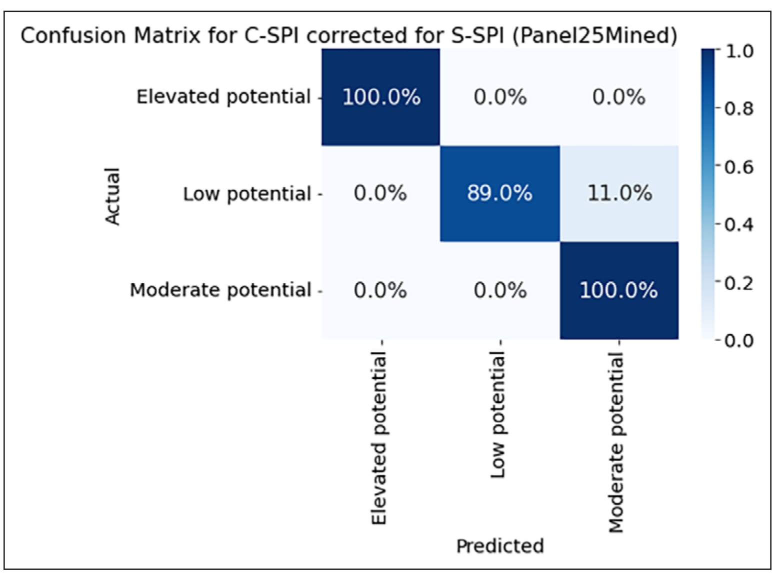

Figure 15. Confusion table after correcting C-SPI for S-SPI

potential during the mining operation. The analyses for this case study showed that anomalous seismic events occur when conditions for unstable sliding along bedding planes are mutually satisfied with conditions for unstable crushing of strata. This understanding led to developing a seismic potential map capable of forecasting 100% of the regions with elevated and moderate seismic potential with no false positive forecasts on elevated potential zones. However, the SPF methodology needs evaluation to be applicable to other mines or other coal basins. This is because the mechanism for induced seismicity can differ from basin to basin. For example, the mechanism behind releasing the energy can be different for the mines in the Uinta basin and those in the Central Appalachian basins. In the Uinta basin, mines might face overstressed coal pillars where coal is competent enough to store strain energy and fail in an unstable manner, while in Central Appalachian mines, unstable sliding along bedding planes might lead to de-confinement of roof strata and thus an unstable collapse of the main roof causing seismicity.

CONCLUSION

This work is a part of an ongoing research program in NIOSH for developing the SPF methodology to reduce risk associated with induced seismicity in longwall mining with different geology conditions. The objective of this paper was to investigate how much accuracy can be obtained in forecasting induced seismic events in a longwall mine in Virginia using a 3D elastic geomechanical model. The hypothesis was that slip-type and compressive-type seismic potential must coincide for an anomalous event to occur during mining. Seismic potential maps were developed using the SPF methodology for both slip-type and compressive-type seismic potential in a district with a history of seismic activity in the mine.

Results showed that when combining SPI of both slip-type and compressive-type events, the location and timing of events in elevated-potential zones and moderate-potential zones were correctly forecasted. No false negative forecasts were reported. There was a false positive forecast in one category: 11% of zones within low-potential regions were forecasted to be moderate-potential zones. With this confirmation of using the SPF for developing seismic potential maps, the next step of this research is to evaluate the performance of the SPF in advance of mining in a district with a different layout design in the study mine.

DISCLAIMER

The findings and conclusions in this report are those of the author(s) and do not necessarily represent the official position of the National Institute for Occupational Safety and Health, Centers for Disease Control and Prevention (CDC). Mention of any company or product does not constitute endorsement by NIOSH.

REFERENCES

Dolinar, Dennis R. (2004). Analysis of the variation of horizontal stresses and strains in bedded deposits in the eastern and Midwestern United States. *Graduate Theses, Dissertations, and Problem Reports*. 1425. In: West Virginia University https://researchrepository.wvu.edu/etd/1425.

Mark, C. and Gadde, M. (2008). Global Trends in Coal Mine Horizontal Stress Measurements. Proceedings, 27th International Conference on Ground Control in Mining, Morgantown, WV, pp. 319–331.

Englund, K. J., & Briggs, G. (1974). Sandstone Distribution Patterns in the Pocahontas Formation of Southwest Virginia and Southern West Virginia. In *Carboniferous of the Southeastern United States* (Vol. 148, pp. 0): Geological Society of America.

Datamine. (2021). https://www.dataminesoftware.com. Retrieved from https://www.dataminesoftware.com/solutions/minescape-geological-modelling-mine-planning/

Itasca. (2016). Itasca Consulting Group Inc..UDEC (universal distinct element code). Minneapolis, USA.: Itasca Consulting Group Inc. Retrieved from https://www.itascacg.com/

Garvey, R. J. (2013). Study of unstable rock failures using finite difference and discrete element methods, Ph. D. dissertation. In: Colorado School of Mines. Arthur Lakes Library. https://hdl.handle.net/11124/78769.

Khademian, Z., & Ozbay, U. (2018). Computational framework for simulating rock burst in shear and compression. *International Journal of Rock Mechanics and Mining Sciences, 110*, 279–290. doi:10.1016/j.ijrmms.2018.06.022

Castro, L. B., Bewick, R., & Carter, T. (2012). *An overview of numerical modelling applied to deep mining. Innovative Numerical Modelling in Geomechanics.* CRC Press. ISBN 9780429212987

Khademian, Z., Van Dyke, M. A., Beale, J., & Wickline, J. (2023). Investigation of Parameters Affecting Seismic Potentials in a Deep Longwall Mine. Proceedings, 57th U.S. Rock Mechanics/Geomechanics Symposium, paper 2023- 0434

Molinda, G. M. (2003). Geologic hazards and roof stability in coal mines. Information circular (National Institute for Occupational Safety and Health); IC 9466;DHHS publication ; no. (NIOSH) 2003-152; URL : https://stacks.cdc.gov/view/cdc/6555

Mitri, H. S., Tang, B., Comeau, W., & Mohammed, M. M. (1999). 3-Dimensional Modelling of Mining Induced Seismic and Strain Energy Parameters. In the proceeding of the 9th ISRM Congress.

Ryder, J. A. (1988). Excess shear stress in the assessment of geologically hazardous situations. *Journal of The South African Institute of Mining and Metallurgy, 88*, 27–39.

Salamon, M. D. G. (1970). Stability, instability and design of pillar workings. *International Journal of Rock Mechanics and Mining Sciences & Geomechanics Abstracts, 7*(6), 613–631. doi:10.1016/0148-9062(70)90022-7

Van Dyke, M., Klemetti, T., Khademian, Z. et al. (2023). Evaluation of Seismic Potential in a Longwall Mine with Massive Sandstone Roof Under Deep Overburden: an Update. *Mining, Metallurgy & Exploration* **40**, 1523–1533. doi:10.1007/s42461-023-00818-x

PROCEEDINGS OF THE 43rd International Conference ON GROUND CONTROL IN MINING

ICGCM 2024

Edited by

Ted Klemetti | Rudrajit Mitra | Michael Murphy | Kyle Perry | Ihsan Berk Tulu

SME
Society for Mining, Metallurgy & Exploration®

Society for Mining, Metallurgy & Exploration (SME)
12999 E. Adam Aircraft Circle
Englewood, Colorado, USA 80112
(303) 948-4200 / (800) 763-3132
www.smenet.org

The Society for Mining, Metallurgy & Exploration (SME) is a professional society whose more than 15,000 members represents all professionals serving the minerals industry in more than 100 countries. SME members include engineers, geologists, metallurgists, educators, students and researchers. SME advances the worldwide mining and underground construction community through information exchange and professional development.

ebook ISBN 978-0-87335-516-2